nature photonics

LETTERS

PUBLISHED ONLINE: 14 AUGUST 2017 | DOI: 10.1038/NPHOTON.2017.139

Variable potentials for thermalized light and coupled condensates

David Dung, Christian Kurtscheid, Tobias Damm, Julian Schmitt, Frank Vewinger, Martin Weitz* and Jan Klaers*†

Quantum gases in lattice potentials have been a powerful platform to simulate phenomena from solid-state physics, such as the Mott insulator transition[1]. In contrast to ultracold atoms, photon-based platforms, such as photonic crystals, coupled waveguides or lasers, usually do not operate in thermal equilibrium[2–5]. Advances towards photonic simulators of solid-state equilibrium effects include polariton lattice experiments[6–10], and the demonstration of a photon condensate[11,12]. Here, we demonstrate a technique to create variable micropotentials for light using thermo-optic imprinting of a dye–polymer solution within an ultrahigh-finesse microcavity. We study the properties of single- and double-well potentials, and find the quality of structuring sufficient for thermalization and Bose–Einstein condensation of light. The investigation of effective photon–photon interactions along with the observed tunnel coupling between sites makes the system a promising candidate to directly populate entangled photonic many-body states. The demonstrated scalability suggests that thermo-optic imprinting provides a new approach for variable microstructuring in photonics.

Periodic potentials for light are at the core of proposals for Mott insulator physics for light, topological effects and driven-dissipative phase transitions[13–18]. Exciton-polariton experiments, involving mixed states of matter and light under conditions of strong coupling, have used permanent semiconductor microstructuring, such as molecular beam epitaxy, metal depositing techniques and mirror patterning[19,20], to demonstrate double-well and periodic potentials[6–9]. In the regime of weak light–matter coupling, thermalization and Bose–Einstein condensation of a photon gas have been achieved in a high-finesse microcavity containing dye molecules in liquid solution[11,12].

Here, we demonstrate a microstructuring technique that allows the generation of variable potentials for light within an optical high-finesse microcavity. The long photon lifetime enables the thermalization of photons and the demonstration of a microscopic photon condensate in a single localized site. We observe effective photon interactions as well as tunnel coupling between two microsites. The associated hybridization of eigenstates of the double-well system is monitored spectroscopically.

The scheme for thermo-optic imprinting of potentials is shown in Fig. 1a. Within a microcavity of finesse near 35,000, variations of the refractive index are induced through irradiation with a laser beam inducing heat from absorption in a 30-nm-thick silicon layer below one of the mirror surfaces. A thermosensitive polymer (poly(*N*-isopropylacrylamide))[21], which undergoes a reversible phase transition to a phase with higher refractive index[22] when heated above 305 K within a narrow temperature range of 0.2 K, is added to the dye solution between the mirrors. Local heating correspondingly increases the optical length between the mirror surfaces, which is equivalent to a local potential drop for a photon gas in the paraxial limit[11]. This can be understood from the larger optical wavelength, corresponding to a smaller photon energy, required to locally match the mirrors' boundary conditions. Transverse temperature patterns within the dye–polymer film are created by scanning a focused laser beam with a two-dimensional galvo scanner over the absorbing silicon coating, while an acousto-optic modulator allows for intensity control, making the technique useful for the creation of variable potentials for light.

Thermalization of the photon gas confined in the microcavity is achieved similarly as described previously[11]. Briefly, the short mirror spacing effectively leads to a low-frequency cutoff for the photon gas. By repeated absorption and re-emission processes on the dye molecules, photons thermalize to the rovibrational temperature of the dye, which is near room temperature. As the spacing between longitudinal modes is of the order of the emission width of the dye (rhodamine in water solution), the thermalization process leaves the longitudinal mode number constant. Correspondingly, the photon gas is effectively two-dimensional, with only transverse modal quantum numbers varied.

The dye solution is pumped with a beam near 532-nm wavelength, chopped to 1-μs pulses with a 50-Hz repetition rate, to reduce the effects of pumping into dye triplet states. The pulse length is more than two orders of magnitude above the thermalization time[23]. As an example for the achieved spatial structuring of the confined photon gas in the thermo-optically imprinted potential, Fig. 1b shows the cavity emission for periodic patterns (left and middle) and a non-periodic pattern (right).

First, we investigated thermalization of the photon gas in a single microtrap. The top panel of Fig. 2a shows typical spectra of the emission of such a microsite for a low-frequency cutoff wavelength of 595 nm and different photon numbers in the cavity. The depth of the potential is h7.5 THz, corresponding to $1.21k_BT$ at $T = 305$ K, where k_B is the Boltzmann constant, and the observed mode spacing is $\Omega/2\pi \cong 1.18$ THz near the trap bottom, which reduces for the higher transverse modes due to deviations from a two-dimensional harmonic oscillator potential. In the thermalized case, we expect the mode spectrum to be Bose–Einstein distributed following

$$n(u_i) = \frac{g(u_i)}{\exp\left(\frac{u_i - \mu}{k_B T}\right) - 1}$$

where u_i (with $u_i = i\hbar\Omega$ for a harmonic potential) denotes the excitation energy of the ith trap level with respect to the low-frequency cutoff, μ is the chemical potential and $g(u_i) = 2(i + 1)$ is the

Institut für Angewandte Physik, Universität Bonn, Wegelerstr. 8, 53115 Bonn, Germany. †Present address: Institute for Quantum Electronics, ETH Zürich, Auguste-Piccard-Hof 1, 8093 Zurich, Switzerland. *e-mail: martin.weitz@uni-bonn.de; jklaers@phys.ethz.ch

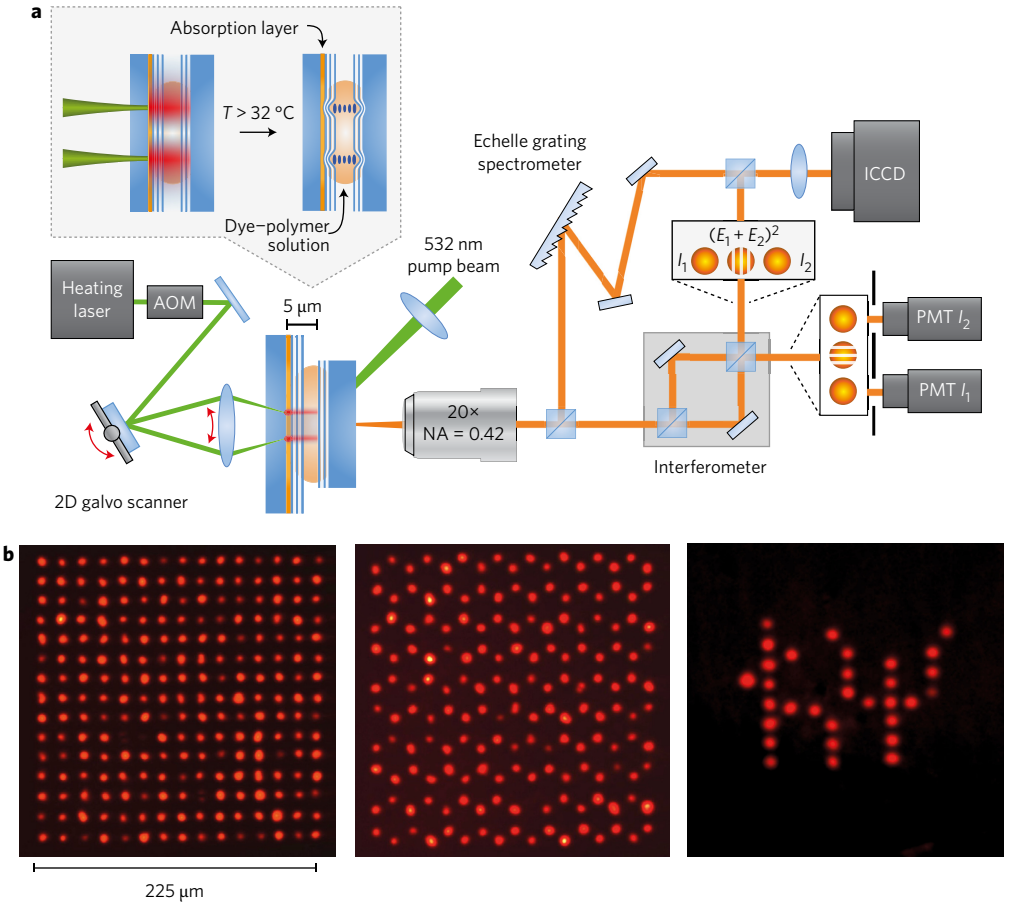

Figure 1 | Set-up and lattice realizations. a, Experimental approach to realize variable potentials for photons within a high-finesse microcavity. Optical radiation is absorbed in a thin silicon layer placed below one of the cavity mirror's dielectric coatings. The induced heat locally increases the index of refraction of the dye-polymer solution within the microcavity, and enhances the optical length. This results in an effective local attractive potential for the photon gas. Complex trapping potentials are realized by scanning an external 'heating' laser beam to imprint the desired transverse temperature modulation onto the absorbing silicon layer. The microcavity is pumped from the reverse side, and its emission can be analysed spatially, interferometrically and spectrally. AOM, acousto-optic modulator. PMT, photomultiplier tube; ICCD, intensified CCD camera; I_1, I_2, optical intensities; E_1, E_2 corresponding field amplitudes. **b**, Experimentally observed images of the microcavity emission for the photon gas in lattices with rectangular (left) and hexagonal (middle) geometry, respectively, and a non-periodic pattern showing the letters 'ħΨ' (right).

degeneracy. The bottom panel of Fig. 2a gives spectrally binned data, yielding the trap levels' population, which agrees well with the predictions within experimental uncertainties. We observe a spectrally broad thermal cloud above the low-frequency cutoff, where above a critical photon number, a Bose–Einstein condensed peak at the position of the cutoff emerges. The observed critical photon number of 67.8(1.6) is three orders of magnitude lower than in previous work with 'macroscopic' photon traps[11], and within uncertainties agrees with the expected value $N_c = 67.5$ (see Methods). The observation of thermalized spectra shows that in photon microtraps loss through, for example mirror transmission, can be kept sufficiently low that within the cavity lifetime photons relax to a near equilibrium distribution. The observed condensate diameter of ~3 µm is close to the harmonic oscillator ground mode size, and we typically use a 15-µm pump beam diameter. For the future, such photon microcondensates are expected to be attractive systems to study few-particle physics effects[24].

To investigate the effect of thermo-optic interactions induced by both the pump beam and condensate photons[11,25,26], as understood for example from residual non-radiative decay channels of excited dye molecules, we have temporally resolved the microcavity emission frequency during a pump pulse (Fig. 2b). We observe an increasing blue-shift of the condensate frequency, corresponding to a decreasing refractive index of the dye–polymer solution. As the temperature increases during the pump pulse, we conclude that the effective thermo-optic coefficient dn/dT is negative. The polymer in steady state has a positive thermo-optic coefficient, but due to the slow (~500 ms) timescale of its response on the 1 µs short timescale of a pump pulse the thermo-optic properties of the water solvent (with $dn/dT < 0$) dominate. Additionally, we have characterized the self-interaction of the condensate by measuring the variation of the mode diameter during one pulse (Fig. 2c). We observe an increase in diameter, and for sufficiently large pump laser spots, this variation becomes independent of details of the pump geometry, and therefore can be attributed to condensate self-interactions. Using a Gross–Pitaevskii model for the retarded thermo-optic effect, we derive a self-interaction parameter of $g_{\mathrm{eff}} = 2.5(8) \times 10^{-5}$ accumulated during 1 µs from our data (see Methods), which is even smaller than previously reported for a rhodamine–methanol medium[11].

To study tunnelling, we employed double-well potentials with a typical spacing between microsites of 8–15 µm. The potentials are prepared with a well depth so shallow that only a single mode is trapped, of frequencies ω_1, ω_2 for the two microsites 1, 2, respectively. One of the sites, say site 1, is pumped, and we slightly red-shift the initial emitter frequency of this pumped site with respect

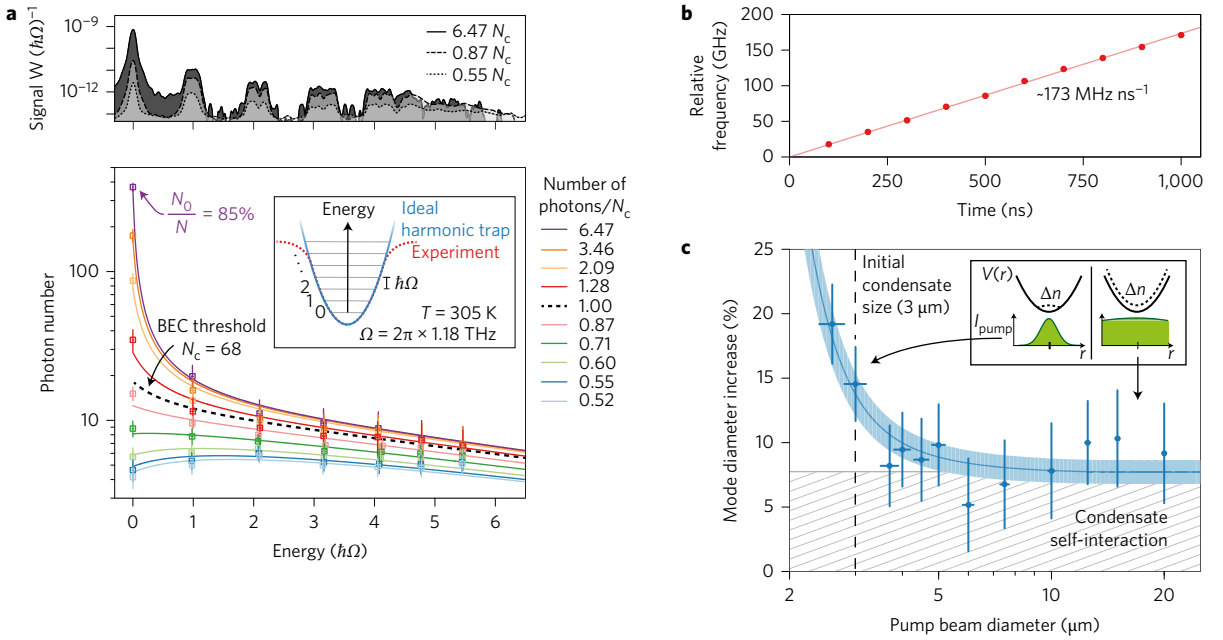

Figure 2 | Thermalization, condensation and photon self-interactions in a single microsite. a, Top: spectrometer data analysing the microcavity emission for different photon numbers in units of the critical photon number, N_c. Bottom: spectrally binned data accounting for the outcoupling mirror transmission to yield the trap level populations (dots), together with theoretical expectations (lines). We observe a spectrally sharp condensate peak at the position of the cavity cutoff on top of a broad thermal cloud distributed over all bound seven trap levels. For the higher trap levels, the level spacing reduces due to deviations from harmonic trapping (see inset). BEC, Bose–Einstein condensate. **b**, Relative emission frequency of the dye microcavity versus time, showing a linear chirp attributed to thermal lensing induced predominantly from the pump beam. The 1-μs duration of the used pump pulses is below the thermal time constant so that no saturation of the chirp is visible (see Methods). These data were recorded for a single microsite, but with the same pump geometry as used for the measurements shown in Figs 3 and 4. **c**, Observed condensate mode size within a pump pulse versus diameter of the pump beam. The photon number in the condensate mode is kept constant for all measurements by adjustment of the pump beam power. The broadening observed for small pump spot diameters of size comparable to the ground mode is attributed to heating directly from the pump beam. For larger diameters, the variation of the optical cloud diameter becomes independent from the pump diameter, as well understood from thermo-optic interactions due to condensate photons. The latter effect is due to heating in the course of the absorption–re-emission cycles of the dye in the presence of the finite quantum efficiency. A Gross–Pitaveskii equation model is used to describe the findings (see Methods). Inset: I_{pump}, pump beam intensity; $V(r)$, potential. All error bars show standard deviations.

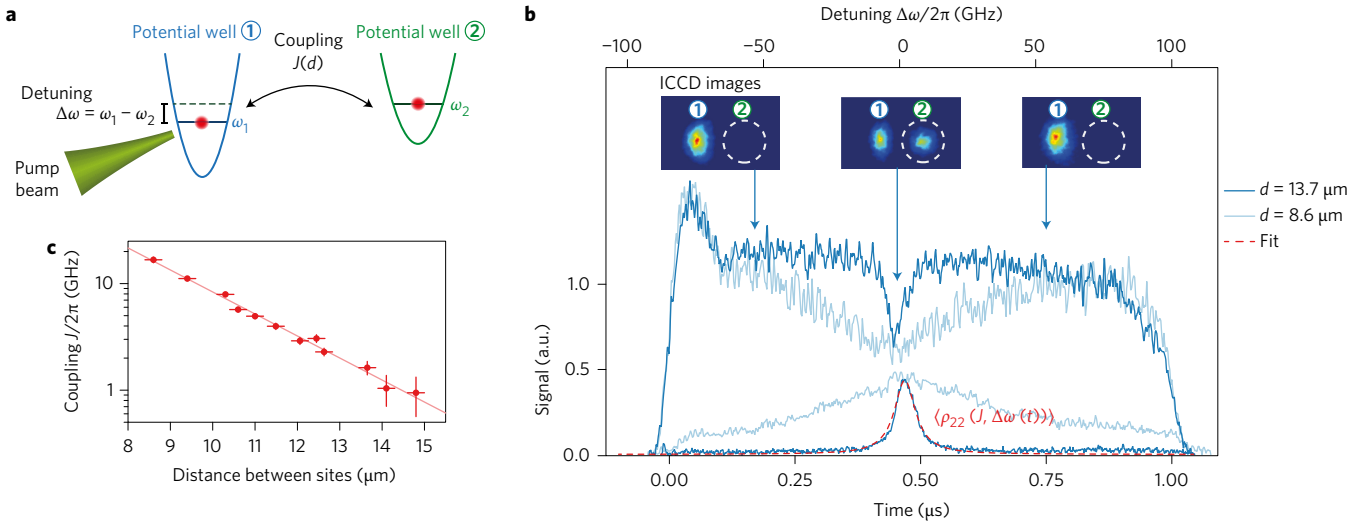

Figure 3 | Tunnelling between two microsites. a,**b**, Schematic of the coupling and time dependence of the emission observed from microsite 1 (top curves in **b**) and site 2 (bottom curves in **b**) for a spacing of 13.7(2) μm (dark blue lines) and 8.6(2) μm (light blue lines), respectively. As the mode energy of the pumped site 1 increases due to thermo-optic effects, the two trap levels align in energy and photons tunnel between sites. Note that the 230-MHz bandwidth of the used photomultiplier detector is not sufficient to resolve temporal oscillations between sites. In **b**, the top scale gives the corresponding detuning between sites assuming a linear chirp of the mode frequency of site 1 with time, see the measurement shown in Fig. 2b. The insets show camera images recorded at corresponding times. **c**, Extracted tunnel coupling versus distance between microsites (dots) with standard deviation (error bars), along with a fit of an exponentially decaying curve (solid line).

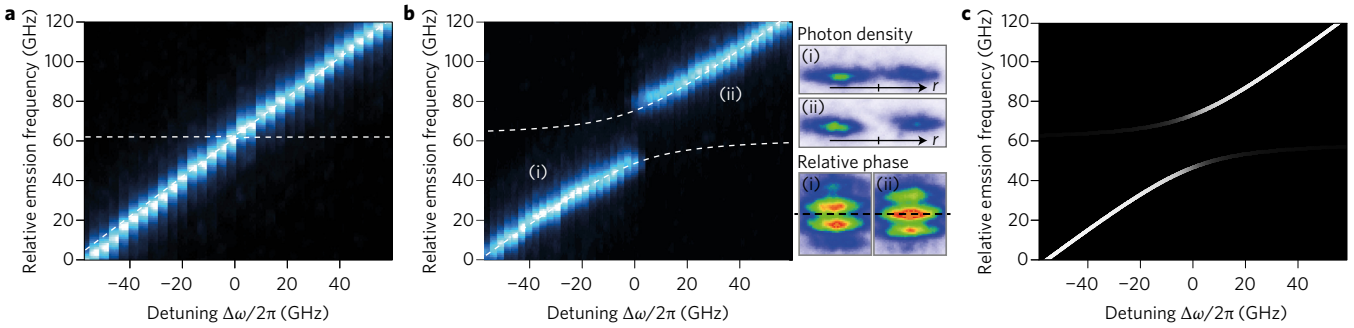

Figure 4 | Eigenstate hybridization in a double-well. a,**b**, Spectra of microcavity emission of site 1 versus the detuning between the sites for a tunnel coupling of $J/2\pi = 1.7$ GHz (**a**) and $J/2\pi = 16.7$ GHz (**b**). The experiment was realized with a spectrometer operating in a gated mode with a 20-ns-long detection period using repeated scans with a variable position of the gate. The dashed lines show the expected location of dressed eigenstates for the corresponding coupling. In **b**, shown on the top right are camera images for the emission in both sites for a detuning of site 1 below (i) and above (ii) that of site 2, and the bottom images show the corresponding interferometer signals. **c**, Theoretical prediction for the emission from site 1 for a $J/2\pi = 16.7$ GHz tunnel coupling between sites in the absence of losses.

to that of site 2, so that during the pump pulse the thermo-optic effect induced by the pump beam will tune the sites into resonance (Fig. 3a). Corresponding data for the time-resolved fluorescence emitted from the individual microsites is shown in Fig. 3b. As the sites are tuned into resonance, we observe tunnelling between microsites, with the number of tunnelled photons again decreasing when the sites shift out of resonance. The resonance width increases for a reduced spacing between sites, as understood from the larger tunnel coupling. The coupling strength derived from the width of the resonance (see Methods) shown in Fig. 3c follows the expected exponential scaling with the distance between microsites. At the smallest investigated distance near 8 μm, the tunnel coupling reaches a value of 16.7(1.1) GHz. The influence of the coupling on the emission frequency was explored by time-resolved spectroscopy of the emission from site 1 during the frequency chirp caused by the thermo-optic effect. Figure 4a was recorded for a tunnel coupling between sites of $J/2\pi = 1.7$ GHz, where no coupling-induced splitting of eigenstates is resolved, while the measurement shown in Fig. 4b gives data for $J/2\pi = 16.7$ GHz, where a clear splitting is visible. The emission frequencies follow well the expectations for an avoided crossing with the corresponding coupling (dashed lines), as readily obtained when modelling the double-well system with a set of coupled Schrödinger equations[27]:

$$i\hbar\,\dot{\psi}_1 = \hbar\,\omega_1 \cdot \psi_1 + \hbar J \cdot \psi_2$$

$$i\hbar\,\dot{\psi}_2 = \hbar J \cdot \psi_1 + \hbar\,\omega_2 \cdot \psi_2$$

where $\psi_{1,2}$ denote optical wavefunctions in the corresponding sites. The eigenstates of the coupled system are $\psi_+ = (\sin(\theta)\psi_1 + \cos(\theta)\psi_2)$, $\psi_- = (\cos(\theta)\psi_1 - \sin(\theta)\psi_2)$, with eigenenergies $E_\mp = \hbar(\omega_1+\omega_2)/2 \pm \sqrt{(\hbar\Delta\omega/2)^2 + J^2}$, where $\theta = \arctan(-2J/\Delta\omega)/2$ denotes the mixing angle and $\Delta\omega = \omega_1 - \omega_2$. Figure 4c gives the expected emission signal $\propto |\langle\psi_\pm|\psi_1\rangle|^2$ from site 1 for $J/2\pi = 16.7$ GHz versus the detuning. The experimental data of Fig. 4b indicates a further suppression of the emission on the weaker side of the two branches where the eigenstates mostly overlap with the unpumped site, an issue attributed to photon losses.

Figure 4b (top right) shows camera images of the emission of the double-well system for mode frequencies of site 1 below (top) and above (bottom) that of site 2. For the former case, (i), we observe a non-vanishing emission in the region between sites (in the classically 'forbidden' region), indicating that the system here is in the symmetric eigenstate ψ_+, while in the latter case, (ii), no emission is observed in that region, as expected for photons in the antisymmetric state ψ_-. When spatially overlapping the emission of the two microsites, the observed fringe pattern shifts by π in phase when tuning from below to above the tunnelling resonance (from case (i) to (ii)). Figure 4b (bottom right) shows the different phase factors of symmetric and antisymmetric eigenstates, respectively, of the 'photonic molecule', which are in good agreement with expectations.

To conclude, we have demonstrated variable potentials for light in an ultrahigh-finesse optical cavity generated using thermo-optic imprinting, a technique compatible with thermal equilibration. A microscopic photon Bose–Einstein condensate with a critical photon number of 68 was observed in a single microtrap. Effective photon interactions as well as photon tunnelling and hybridization of eigenstates in a double-well potential has been achieved.

For the future, we expect novel applications of thermo-optic patterning within low-loss resonators in other fields of photonics as well. Prospects of photon condensates in lattice potentials include the population of entangled states[5,28]. Unlike in ultracold gas systems[1], loading and cooling in our system proceeds throughout the lattice manipulation time, and when constituting the system ground state, quantum many-body states can be populated in a thermal equilibrium process.

Methods

Methods and any associated references are available in the online version of the paper.

Received 22 December 2016; accepted 13 July 2017; published online 14 August 2017

References

1. Bloch, I., Dalibard, J. & Zwerger, W. Many-body physics with ultracold gases. *Rev. Mod. Phys.* **80,** 885–964 (2008).
2. Fleischer, J. W., Segev, M., Efremidis, N. K. & Christodoulides, D. N. Observation of two-dimensional discrete solitons in optically induced nonlinear photonic lattices. *Nature* **422,** 147–150 (2003).
3. Schwartz, T., Bartal, G., Fishman, S. & Segev, M. Transport and Anderson localization in disordered two-dimensional photonic lattices. *Nature* **446,** 52–55 (2007).
4. Nixon, M., Ronen, E., Friesem, A. A. & Davidson, N. Observing geometric frustration with thousands of coupled lasers. *Phys. Rev. Lett.* **110,** 184102 (2013).
5. Carusotto, I. & Ciuti, C. Quantum fluids of light. *Rev. Mod. Phys.* **85,** 299–366 (2013).
6. Lai, C. W. *et al.* Coherent zero-state and π-state in an exciton–polariton condensate array. *Nature* **450,** 529–532 (1997).
7. Lagoudakis, K. G., Pietka, B., Wouters, M., André, R. & Deveaud-Plédran, B. Coherent oscillations in an exciton–polariton Josephson junction. *Phys. Rev. Lett.* **105,** 120403 (2010).
8. Jacqmin, T. *et al.* Direct observation of Dirac cones and a flatband in a honeycomb lattice for polaritons. *Phys. Rev. Lett.* **112,** 116402 (2014).

9. Abbarchi, M. *et al.* Macroscopic quantum self-trapping and Josephson oscillations of exciton polaritons. *Nat. Phys.* **9,** 275–279 (2012).
10. Cristofolini, P. *et al.* Optical superfluid phase transitions and trapping of polariton condensates. *Phys. Rev. Lett.* **110,** 186403 (2013).
11. Klaers, J., Schmitt, J., Vewinger, F. & Weitz, M. Bose–Einstein condensation of photons in an optical microcavity. *Nature* **468,** 545–548 (2010).
12. Marelic, J. & Nyman, R. A. Experimental evidence for inhomogeneous pumping and energy-dependent effects in photon Bose-Einstein condensation. *Phys. Rev. A* **91,** 033813 (2015).
13. Hartmann, M. J., Brandao, F. G., & Plenio, M. B. Strongly interacting polaritons in coupled arrays of cavities. *Nat. Phys.* **2,** 849–855 (2006).
14. Greentree, A. D., Tahan, C., Cole, J. H. & Hollenberg, L. C. L. Quantum phase transitions of light. *Nat. Phys.* **2,** 856 (2006).
15. Angelakis, D. G., Santos, M. F. & Bose, S. Photon-blockade-induced Mott transitions and *XY* spin models in coupled cavity arrays. *Phys. Rev. A* **76,** 031805 (2007).
16. Schiro, M., Bordyuh, M., Öztop, B. & Türeci, H. E. Phase transitions of light in cavity QED lattices. *Phys. Rev. Lett.* **109,** 053601 (2012).
17. Umucalilar, R. O. & Carusotto, I. Fractional quantum Hall states of photons in an array of dissipative coupled cavities. *Phys. Rev. Lett.* **108,** 206809 (2012).
18. de Leeuw, A.-W., Onishchenko, O., Duine, R. A. & Stoof, H. T. C. Effects of dissipation on the superfluid–Mott-insulator transition of photons. *Phys. Rev. A* **91,** 033609 (2015).
19. Flatten, L. C., Trichet, A. A. P. & Smith, J. M. Spectral engineering of coupled open-access microcavities. *Laser Photon. Rev.* **10,** 257–263 (2016).
20. Urbonas, D. *et al.* Zero-dimensional organic exciton–polaritons in tunable coupled Gaussian defect microcavities at room temperature. *ACS Photon.* **3,** 1542–1545 (2016).
21. Fujishige, S., Kubota, K. & Ando, I. Phase transition of aqueous solutions of poly (*N*-isopropylacrylamide) and poly(*N*-isopropylmethacrylamide). *J. Phys. Chem.* **93,** 3311–3313 (1989).
22. Ishikawa, M., Misawa, H., Kitamura, N., Fujisawa, R. & Masuhara, H. Infrared laser-induced photo-thermal phase transition of an aqueous poly(*N*-isopropylacrylamide) solution in the micrometer dimension. *Bull. Chem. Soc. Jpn* **69,** 59–66 (1996).
23. Schmitt, J. *et al.* Thermalization kinetics of light: from laser dynamics to equilibrium condensation of photons. *Phys. Rev. A* **92,** 011602 (2015).
24. Chuu, C.-S. *et al.* Direct observation of sub-Poissonian number statistics in a degenerate Bose gas. *Phys. Rev. Lett.* **95,** 260403 (2005).
25. Nyman, R. A. & Szymanska, M. H. Interactions in dye-microcavity photon condensates and the prospects for their observation. *Phys. Rev. A* **89,** 033844 (2014).
26. Van der Wurff, E. C. I., de Leeuw, A.-W., Duine, R. A. & Stoof, H. T. C. Interaction effects on number fluctuations in a Bose-Einstein condensate of light. *Phys. Rev. Lett.* **113,** 135301 (2014).
27. Raghavan, S., Smerzi, A., Fantoni, S. & Shenoy, S. R. Coherent oscillations between two weakly coupled Bose–Einstein condensates: Josephson effects, π oscillations, and macroscopic quantum self-trapping. *Phys. Rev. A* **59,** 620–633 (1999).
28. Klaers, J. *et al.* Bose-Einstein condensation of photons in a microscopic optical resonator: towards photonic lattices and coupled cavities. *Proc. SPIE* **8600,** 86000L (2013).

Acknowledgements

We thank U. Fischer for valuable discussions on the thermal model. Financial support by the Deutsche Forschungsgemeinschaft (Collaborative Research Centre 185) and the European Research Council (Interacting Photon Bose–Einstein Condensates in Variable Potentials—INPEC) is acknowledged.

Author contributions

D.D., C.K., T.D., J.S., F.V. and J.K. analysed the data. D.D., M.W. and J.K. conceived and designed the experiments. D.D., C.K., T.D., J.S. and J.K. contributed materials/analysis tools. D.D., C.K., J.S. and J.K. performed the experiments. D.D., F.V., M.W. and J.K. wrote the paper.

Additional information

Supplementary information is available in the online version of the paper. Reprints and permissions information is available online at www.nature.com/reprints. Publisher's note: Springer Nature remains neutral with regard to jurisdictional claims in published maps and institutional affiliations. Correspondence and requests for materials should be addressed to M.W. and J.K.

Competing financial interests

The authors declare no competing financial interests.

Methods

Experimental set-up and procedure. The used microcavity consists of two highly reflective plane mirrors (specified reflectivity above 99.991% in the spectral range of 520–590 nm wavelength) spaced apart by a distance of $D_0 = 1.98$ μm. We used a plane-mirror microcavity, so that effective trapping potentials for the photon gas are solely due to thermo-optic transverse index variations. The microcavity was filled with a solution of the thermosensitive polymer poly(*N*-isopropylacrylamide) at concentration, $\rho = 8\%$, and rhodamine 6G dye ($\rho = 0.04\%$, corresponding to 10^{-3} mol l^{-1}) dissolved in water and Ammonyx-LO ($\rho = 5\%$) as a surfactant. Water was used as the solvent because the polymer dissolves well in it, despite the smaller quantum efficiency of the rhodamine dye in this environment (≈80%–95%) compared with that obtained when ethylene glycol solvent was used in our earlier experiments[11,23]. Above 32.4 °C, within a temperature range of ≈0.2 °C, the polymer undergoes a phase transition to a globule state with collapsed polymer chains, and the associated molecular transport increases the specified refractive index from $n \approx 1.35$ to $n \approx 1.46$ (ref. 29). We have not seen evidence for a reduction of the cavity finesse caused by the dye–polymer phase transition, which we attribute to the fact that slightly above the phase transition the formed globules for the relevant timescales remain at a relatively small size[30]. The timescale of the refractive index change within the microcavity environment was experimentally determined by monitoring the induced variation of the cavity emission frequency on local heating to be ≈500 ms. Between the glass substrate and the dielectric coating of one of the cavity mirrors a 30-nm-thick silicon coating was placed, which at 532 nm wavelength absorbs 30% of the incident irradiation to convert the transversally spatially modulated optical pattern into a temperature profile. For a numerical simulation of induced temperature distributions see the Supplementary Information, which also shows a predicted temperature gradient along the cavity axis. The temperature pattern is induced by a beam near 532 nm wavelength of 5–15 mW power focused to 2-μm diameter that is scanned transversally with a two-dimensional galvo scanner. This scan was done on a 100-ms timescale, which is fast compared with the mentioned timescale of the polymer phase transition. The beam power is controlled with an acousto-optic modulator. The local variation of the optical length between mirror surfaces induced by the refractive index change leads to a transversally varying potential in the microcavity. Due to the high reflectivity of the dielectric coating, transmission of the auxiliary 'heating' beam into the microcavity is suppressed by four orders of magnitude, allowing for a control of the cavity photon number independently from the 'heating' beam. Photons are injected into the microcavity by pumping with a further laser beam near 532 nm wavelength from the reverse cavity side at ~45° to the optical axis. The typically used pump power is up to 2 W for a 15-μm beam diameter for the single-well measurements shown in Fig. 2a, whereas to pump one site of the double-well measurements shown in Figs 3 and 4, as well for the measurement shown in Fig. 2b, elliptical beams of diameter 3 μm and 20 μm along the short and long axis, respectively, were used.

Photons trapped in the microcavity acquire a thermalized distribution from absorption and re-emission processes on dye molecules, provided that the cavity lifetime exceeds the thermalization time[23,31]. Rapid decoherence from frequent collisions of dye molecules with the solvent prevents a coupling of the phases of dipole and photon[11], so we can assume to be in the weak-coupling regime of photons and molecules. The small spacing, corresponding to 4.5 optical wavelengths in the medium, causes a large frequency spacing between longitudinal cavity modes, comparable to the emission width of the dye. Experimentally, we observe that only photons with fixed longitudinal mode number, $q = 9$, populate the cavity, making the system effectively two-dimensional. This also introduces an effective low-frequency cutoff near $\hbar\omega_{\mathrm{cutoff}} \cong 2.1$ eV, with $\omega_{\mathrm{cutoff}} = 2\pi c/\lambda_{\mathrm{cutoff}}$, $\lambda_{\mathrm{cutoff}} \cong 595$ nm. The pump beam is acousto-optically chopped into 1-μs-long pulses at a typical 50 Hz repetition rate to suppress pumping into dye triplet states. The pulse duration exceeds the thermalization time, which is of order of the 4-ns upper electronic state natural lifetime of the rhodamine dye molecule, or far above the threshold in the picosecond regime[23], by at least two orders of magnitude, that is, from the point of photon gas thermalization the experiment operates in a quasi-continuous-wave mode. The obtained maximum condensate fractions were near 85%, corresponding to the top spectrum shown in the upper and lower panels of Fig. 2a, while at higher photon numbers deviations from equilibrium spectra increase[32].

With the thermo-optic method in the dye–polymer microcavity, potential well depths up to h9.5 THz, corresponding to ~$1.5k_BT$, have been achieved, and trap frequencies $\Omega/2\pi$ of individual microtraps are in the range 0.2 to 2 THz. We have realized trap sizes down to 3 μm diameter, a value attributed to be limited by transverse heat diffusion due to the non-vanishing distance between the silicon heating layer and the dye–polymer solution determined by the thickness of the dielectric mirror layers. The quoted value for the maximum well depth corresponds to a refractive index change $\Delta n \cong 0.04$ (that is, below the expected maximum possible difference of $\Delta n \cong 0.11$, thus reducing effects of saturation) of the thermosensitive polymer at the phase transition. To calculate this value we have assumed that 4.7 half waves are in the dye–polymer solution, whereas 4.3 half waves penetrate into the dielectric coatings of the mirrors[33].

Each data point of the emission spectrum of a single microsite shown in Fig. 2a (top) is the average of 2,000 individual measurement results. The observed spacing between the lowest transverse modes is nearly equidistant, so the generated potential near the trap minimum can be assumed to be harmonic (Supplementary Information). This spacing of $\Omega/2\pi \cong 1.18$ THz, corresponding to the trap vibrational frequency, translates to an effective radius of curvature of the reflecting surfaces of $R_{\mathrm{eff}} = 2c^2/(n^2 D_0 \Omega^2) \cong 0.9$ mm. One can show that the photon gas in a spherically curved mirror resonator is formally equivalent to a two-dimensional gas of harmonically confined, massive particles with an effective mass $m_{\mathrm{ph}} = \hbar\omega_{\mathrm{cutoff}}/(c/n)^2$, for which it is known that a Bose–Einstein condensate exists at thermal equilibrium conditions[11]. The expected critical particle number is

$$N_c = \sum_{u=u_1,u_2,\ldots,u_6} \frac{2(u/\hbar\Omega + 1)}{e^{(u/k_BT)} - 1} \quad (1)$$

which for the above quoted value for Ω and the ambient temperature $T = 305$ K yields $N_c \cong 67.5$. This value is three orders of magnitude below the value reported in our earlier 'macroscopic' photon Bose–Einstein condensation experiment, carried out with two resonator mirrors of 1 m spherical curvature[11]. We note that the experiment reported here operates far from the thermodynamic limit, as there only are 7 eigenenergy levels (corresponding to 56 trapped eigenstates in total, including also the polarization degeneracy). Despite this small number of energy levels, our experimental observations are in good agreement with Bose–Einstein condensation theory. A visible small overpopulation of the higher-order modes for the spectra with low photon numbers is attributed to imperfect spatial filtering of the fluorescent emission from the microsite, causing some stray light from continuum modes in the presence of a finite spectral resolving power to reach the detector. The observed spectral width of the modes (top panel in Fig. 2a) reaches 90 GHz for the ground mode, which is above the 30-GHz resolution of the used spectrometer, and is attributed to the thermo-optic drift during the pump pulse. The broadening of higher trap levels is technical in nature, and attributed to aberrations in the used slitless spectrometer, as understood from an admixture of spatial with spectral information, along with possible contributions of a lift of degeneracy due to deviations from radial symmetry.

The measurements shown in Fig. 2b were recorded by spectrally analysing the emission of a single microsite in a time-resolved way. The intensified CCD camera gate time was varied between 100 ns and 1 μs, and the corresponding variation of the spectra was monitored with an echelle grating spectrometer of 9-GHz spectral resolution. We observe a nearly linear frequency chirp to higher eigenfrequencies which within the pulse time does not approach a steady state. This data were recorded for the same pump beam geometry as used for the measurements shown in Figs 3 and 4, and is attributed to be dominated by thermo-optic effects induced from heating from the pump beam pulse. In the data of Fig. 2b we find a chirp rate of $\mathrm{d}\nu/\mathrm{d}t = 173(4)$ MHz ns^{-1}. This allows to calibrate the time axis shown in the double-well data of Fig. 3b to a frequency axis giving the detuning between sites, as shown on the top of the diagram. The quoted value for the chirp rate can be used to estimate a local heating rate $\mathrm{d}T/\mathrm{d}t$ of the dye–polymer solution during the pump pulse. Here, we arrive at $\mathrm{d}T/\mathrm{d}t = (-1/\kappa) \times n/\nu \times \mathrm{d}\nu/\mathrm{d}t \approx 4.6$ K $\mu\mathrm{s}^{-1}$, where κ denotes the thermo-optic coefficient of water ($\kappa \approx -1 \times 10^{-4}$ 1/K).

The refractive index change due to the polymer phase transition is much larger and of different sign than refractive index variations from the thermo-optic effect in water. The typical timescales are 0.5 s for a refractive index change due to the polymer phase transition and $\tau \approx 4$ μs for the usual thermo-optic effect (τ was evaluated at a few micrometres optical beam diameter). Hence, the transient response is dominated by the latter effect. Note that the timescale of the thermo-optic effect is dependent on the geometry of the system, and increases for larger optical beam sizes. Figure 2b shows the corresponding experimentally observed increase of the condensate frequency within the 1-μs pulse. The conclusion that the transient response is dominated by the thermo-optic effect in water is supported by the fact that within the 1-μs-long pump pulse, we observe for all pump beam diameters (that is, both in the case of the observed thermo-optic effect being dominated by heating from the pump pulse itself and the cavity photons) an increase of the ground mode diameter, as expected for $\mathrm{d}n/\mathrm{d}T < 0$.

The measurements shown in Fig. 2c were conducted to characterize thermo-optic effects in the dye–polymer cavity environment in more detail. For those measurements, potentials with reduced depth were used, so that only a single level was trapped (as for the data shown in Figs 3 and 4). In the experiment, the diameter of the macroscopically occupied mode was measured alternating at the beginning and the end of the 1-μs-long pump pulse, with the gate of the ICCD camera set to 50 ns. The vertical scale gives the observed relative broadening of the emitted condensate mode within a pump pulse. Each data point gives the average of results of 200 individual measurements. The described procedure is carried out for different pump beam diameters, while keeping the photon number in the macroscopically occupied mode fixed ($N_0 = 50{,}000 \pm 4000$). The pump power was increased quadratically with pump beam diameter. We note that due to the presence of only a single trapped level, thermalization was not relevant for this measurement and thus high photon number could be used.

To model the system in the presence of thermo-optic interactions, we started with a two-dimensional Gross–Pitaevskii equation

$$\left(-\frac{\hbar^2\nabla^2}{2m_{\rm ph}}+V(\mathbf{r},t)+E_{\rm int}(\mathbf{r},t)\right)\psi(\mathbf{r},t)=\mu\psi(\mathbf{r},t) \tag{2a}$$

where $V(\mathbf{r},t)$ is an effective trapping potential for photons and μ is the chemical potential. Thermo-optic effects are assumed to be slow with respect to the timescale on which the photon wavefunction reaches a steady state. Correspondingly, equation (2a) has the form of the stationary Gross–Pitaevskii equation with a residual time-dependence due to the slow variation of the thermo-optical self-interaction. The interaction energy due to the refractive index change of the solution from heating through condensate photons can be written as

$$E_{\rm int}\cong -m_{\rm ph}(c/n_0)^2\frac{\Delta n}{n_0} \tag{2b}$$

where n_0 is the refractive index of the solution at temperature T_0 of the mirrors, which are regarded to act as a heat sink. Further, $\Delta n=(\partial n/\partial T)\cdot(T(\mathbf{r};t)-T_0)\equiv A\cdot(T(\mathbf{r},t)-T_0)$, where $\Delta n(\mathbf{r},t)$ and $T(\mathbf{r},t)$ denote the refractive index variation (with $\Delta n\ll n_0$) and temperature, respectively, at the corresponding transverse position averaged over the cavity length, and $A=(\partial n/\partial T)$ is the thermo-optic coefficient of the dye solution. As we do not observe evidence for an (ultrafast) Kerr interaction[11,25,26] at the present level of accuracy with the used solution, no corresponding term is added to equation (2b). In our model, we assume that the temperature profile of the cavity relaxes towards a steady state that is determined by the intensity of the light field on a timescale τ. The corresponding time-evolution of the temperature in the presence of a heating term $B|\psi(\mathbf{r},t)|^2$ is described by

$$\frac{{\rm d}T(\mathbf{r},t)}{{\rm d}t}=-\frac{1}{\tau}\left(T(\mathbf{r},t)-T_0\right)+B\left|\psi(\mathbf{r},t)\right|^2 \tag{2c}$$

and has the formal solution

$$T(\mathbf{r},t)=T_0+B\int_{-\infty}^{t}N_0\left|\psi(\mathbf{r},t')\right|^2e^{-(t-t')/\tau}{\rm d}t' \tag{2d}$$

With the initial condition $|\psi(\mathbf{r},t)|^2\equiv 0$ for $t<0$, we arrive at a Gross–Pitaevskii equation for a temporally retarded interaction term

$$\left(-\frac{\hbar^2\nabla^2}{2m_{\rm ph}}+V(\mathbf{r},t)+\frac{\hbar^2}{m_{\rm ph}}\frac{g_{\rm stat}}{\tau}N_0\int_0^t\left|\psi(\mathbf{r},t')\right|^2e^{(t'-t)/\tau}{\rm d}t'\right)\psi(\mathbf{r},t)=\mu\psi(\mathbf{r},t) \tag{2e}$$

where $g_{\rm stat}=-\tau ABm/\hbar^2$ denotes the dimensionless two-dimensional interaction constant expected at stationary conditions due to thermo-optic self-interactions.

Refractive index changes induced by heating from the pump beam can be accounted for in an analogous way, by first introducing a heating term into equation (2c) that has the spatial transverse profile of the Gaussian-shaped pump beam. We arrive at an extra potential energy $V_{\rm pump}(\mathbf{r},t)=\xi(t)\cdot I_{0,\rm pump}\exp(-2r^2/w_{\rm pump}^2)$, where $I_{0,\rm pump}=2P_{\rm pump}/\pi w_{\rm pump}^2$, with $w_{\rm pump}$ denoting the radius and $P_{\rm pump}$ the power of the pump beam, and ξ is a proportionality factor that for $t\ll\tau$ (similarly as the third term in equation (2e)) scales linearly with the length of the pump pulse. When including a harmonically-shaped photon trapping potential $V_{\rm harmon}(\mathbf{r})=(m_{\rm ph}/2)\Omega^2r^2$, the total trapping potential can be written in the form

$$V(\mathbf{r};t)=V_{\rm trap}(\mathbf{r})+V_{\rm pump}(\mathbf{r},t)\cong\frac{m_{\rm ph}}{2}\Omega'(t)^2r^2+\xi(t)\cdot I_{0,\rm pump} \tag{2f}$$

with $\Omega'(t)=\Omega(1-2\xi(t)\cdot I_{0,\rm pump}/\Omega^2m_{\rm ph}w_{\rm pump}^2)$ for $\Omega'/\Omega\ll 1$.

We next restrict ourselves to the case of times much below the retardation time constant τ and sufficiently small interactions. In this limit, only small modifications of the wavefunction due to interactions are expected, so that the approximation $|\psi(\mathbf{r},t')|^2\cong|\psi(\mathbf{r},0)|^2$ in the interaction term is justified. Correspondingly, this term simplifies to $E_{\rm int}(\mathbf{r},t)=(\hbar^2/m_{\rm ph})g_{\rm eff}(t)N_0|\psi(\mathbf{r},0)|^2$ with the time-dependent effective interaction constant $g_{\rm eff}(t)=(t/\tau)g_{\rm stat}$. In this limit, the problem can for the harmonically trapped case be solved analytically with a variational method, as described in ref. 34. We begin by writing the energy of the system in the functional form

$$E(\psi)=\int{\rm d}\mathbf{r}\left(\frac{\hbar^2}{2m_{\rm ph}}\left|\nabla\psi(\mathbf{r},t)\right|^2+V(\mathbf{r},t)\left|\psi(\mathbf{r},t)\right|^2+\frac{1}{2}\frac{\hbar^2}{m_{\rm ph}}g_{\rm eff}(t)N_0^2\left|\psi(\mathbf{r},t)\right|^4\right) \tag{2g}$$

Note that minimization of $(E-\mu N_0)$ with respect to ψ^* at a fixed value of the chemical potential μ gives the Gross–Pitaevskii equation of equation (2e). To find the condensate wavefunction, we use a Gaussian trial function of width $w=w_{0,\rm cond}+\Delta w_{\rm cond}$, where $w_{0,\rm cond}$ denotes the width of the harmonic oscillator wavefunction (as obtained with no interactions), and minimize the energy in the presence of interactions with respect to variations in w. When also accounting for the above described thermo-optic effects induced by the pump beam, we find a relative broadening of the condensate diameter of

$$\frac{\Delta w_{\rm cond}}{w_{0,\rm cond}}\cong\frac{\xi\cdot P_{\rm pump}}{\Omega^2m_{\rm ph}^2\pi w_{\rm pump}^4}+\frac{N_0}{8\pi}\cdot g_{\rm eff}(t) \tag{2h}$$

where we have assumed $\Delta w_{\rm cond}\ll w_{\rm cond}$. The first term is due to thermo-optic effects induced directly by heating from the pump beam, which rapidly decays with increased pump beam diameter. The contribution from photon self-interactions can then readily be identified from the asymptotic value at large pump beam diameters, which is described by the second term (as indicated by the hatched area in Fig. 2c). In contrast to the Thomas–Fermi regime (interaction energy dominating over kinetic energy), for which in two-dimensional systems the condensate diameter scales with $(N_0)^{1/4}$, the system presented here with $\Delta w_{\rm cond}\ll w_{\rm cond}$ is in the opposite regime of the kinetic energy dominating over the interaction energy, for which one finds a linear increase of the condensate diameter with particle number N_0. For an experimental investigation of this scaling, see the Supplementary Information.

At the used $t=1$ µs thermo-optic interaction time, corresponding to the length of a pump pulse, the observed asymptotic value of the condensate mode broadening at large pump beam diameter, see also Fig. 2c, reaches 8(1)%. Using equation (2h) we derive an accumulated effective interaction constant $g_{\rm eff}=4(2)\times10^{-5}$. In addition to the described analytic estimation, we have also performed a full numeric evaluation of the Gross–Pitaevskii equation, from which we find a numeric value of the interaction constant of $g_{\rm eff}=2.5(8)\times10^{-5}$ for the observed condensate broadening. The latter value corresponds to a static interaction constant $g_{\rm stat}=(\tau/t)\cdot g_{\rm eff}=1.0(3)\times10^{-4}$, when using the above quoted value of a $\tau=4$ µs thermal time constant. These quoted values for the dimensionless interaction constant are below that reported in earlier experiments of our group for a different experimental situation[11], as understood mainly (i) from the use of water as a solvent in the present experiment with its comparatively low thermo-optic coefficient, (ii) the cutoff being at a relatively long wavelength resulting in a small photon absorption rate, and (iii) the here quoted value of $g_{\rm eff}$ referring to the influence of the thermo-optic interaction during a single pump pulse.

The tunnelling couplings J between potential wells were determined from the spectra shown in Fig. 3b using a Bloch equation model accounting for a pump rate λ of site 1 and a loss rate Γ:

$$\dot\rho_{11}=\lambda-\Gamma\rho_{11}-2J{\rm Im}(\rho_{12}) \tag{3a}$$

$$\dot\rho_{22}=-\Gamma\rho_{22}+2J{\rm Im}(\rho_{12}) \tag{3b}$$

$$\dot\rho_{12}=-(\Delta\omega+\Gamma)\rho_{12}-iJ{\rm Im}(\rho_{22}-\rho_{11}) \tag{3c}$$

where ρ_{11}, ρ_{22} denote the populations in sites 1,2, respectively, ρ_{12} $(=\rho_{21}^*)$ the corresponding off-diagonal matrix element, and $\Delta\omega=\omega_1-\omega_2$. One finds the stationary analytic solutions

$$\rho_{11}^{\rm stat}=\frac{\lambda}{\Gamma}\left(1-\frac{2J^2}{\Delta\omega^2+\Gamma'^2}\right) \tag{4a}$$

$$\rho_{22}^{\rm stat}=\frac{\lambda}{\Gamma}\cdot\frac{2J^2}{\Delta\omega^2+\Gamma'^2} \tag{4b}$$

$$\rho_{12}^{\rm stat}=\frac{-i\Gamma-\Delta\omega}{\Delta\omega^2+\Gamma^2}\cdot2\left(\rho_{22}^{\rm stat}-\rho_{11}^{\rm stat}\right) \tag{4c}$$

with the saturation broadened resonance width $\Gamma'=\sqrt{\Gamma^2+4J^2}$.

From the observed value for the resonant tunnelling ratio for the spectra as shown in Fig. 3b we determined the ratio J/Γ of tunnel coupling and loss rate using the expected ratio $\rho_{11}(\Delta\omega=0)/\rho_{11}(\Delta\omega\to\infty)=1-1/[2(1+(\Gamma/2J)^2)]$ for each spectrum of a certain distance between microsites. This allowed us in the next step to determine the corresponding value for the tunnel coupling J from the fitted width of the spectra (Fig. 3c). This readily also allowed us to determine the loss rate, and after averaging over the results of the different spectra a value $\Gamma=11(5)$ GHz was obtained.

The spectral data shown in Fig. 4a,b was obtained by using a gated ICCD camera detector (20 ns gate time) monitoring the emission after the echelle monochromator to analyse the microcavity emission. Such measurements were repeated for different delay times after the onset of the pump pulse to allow for the analysis of the temporal variation of the microcavity emission during the frequency chirp of the detuning of microsite 1 relative to site 2 from the thermo-optic effect. The expected value for the population of dressed eigenstates of the double-well system shown in Fig. 4c was derived from projecting the eigenstates of the system onto the left well (site 1). This method gives the expected value for the relative values of the emission of the two sites in the absence of losses.

Data availability. The data that support the plots within this paper and other findings of this study are available from the corresponding authors upon reasonable request.

References

29. Reufer, M., Dıaz-Leyva, P., Lynch, I. & Scheffold, F. Temperature-sensitive poly (*N*-isopropyl-acrylamide) microgel particles: a light scattering study. *Eur. Phys. J. E* **28,** 165–171 (2009).
30. Inoue, H. *et al.* Conformational relaxation dynamics of a poly(*N*-isopropylacrylamide) aqueous solution measured using the laser temperature jump transient grating method. *Phys. Chem. Chem. Phys.* **14,** 5620–5627 (2012).
31. Kirton, P. & Keeling, J. Nonequilibrium model of photon condensation. *Phys. Rev. Lett.* **111,** 100404 (2013).
32. Marelic, J. *et al.* Spatiotemporal coherence of non-equilibrium multimode photon condensates. *New J. Phys.* **18,** 103012 (2016).
33. Klaers, J. *et al.* Bose–Einstein condensation of paraxial light. *Appl. Phys. B* **105,** 17 (2011).
34. Pethick, C. J. & Smith, H. *Bose–Einstein Condensation in Dilute Gases* (Cambridge Univ. Press, 2008).